Humidity responsive actuation of bioinspired hygromorph biocomposites (HBC) for adaptive structures

Antoine Le Duigou, Vincent Keryvin, Johnny Beaugrand, Miguel Pernes, Fabrizio Scarpa, Mickael Castro

Humidity responsive actuation of bioinspired hygromorph biocomposites (HBC) for adaptive structures

Antoine Le Duigou[a], Vincent Keryvin[a], Johnny Beaugrand [b,c], Miguel Pernes[b], Fabrizio Scarpa[d] and Mickael Castro[a]

[a] Univ. Bretagne Sud, UMR CNRS 6027, IRDL, F-56100 Lorient, France

[b] INRA, UMR614 FARE, Fractionnement des AgroRessources et Environnement, 2 esplanade Roland Garros, F-51100 Reims, France

[c] INRA, Research Unit BIA UR1268, Rue Géraudiere, F-44316 Nantes, France

[d] Bristol Composites Institute (ACCIS), University of Bristol, BS8 1TR Bristol, UK

Abstract

Hygromorph biocomposites (HBC) possess moisture-induced actuation from bioinspired designs. The present work describes a large experimental and comprehensive database of the hygro-mechanical and bending actuation properties of flax/maleic anhydride grafted polypropylene (MAPP) HBC composites over a large range of moisture variation (10-90% RH) and water immersion. HBCs exhibit a promising responsiveness and reactivity over the whole relative humidity range (10-90% RH), with acceleration and increase of the actuation observed as soon as a 30% RH value is reached. The experimental data are compared to analogous results from an analytical model based on a modified Timoshenko theory, and a finite element model based on the use of classical laminate theory (CLT). We discuss the effects of the hygroscopic properties (β coefficient) and the design parameters (length/width and thickness ratios) of the composites on the actuation performance.

Keywords : Biocomposite, Smart materials, Moisture, Mechanical properties

1 Introduction

Bioinspired design is a source of creativity for designers, engineers and scientists. Nature suggests several ways on how function/microstructure/material relationships and material hierarchy could be

used in technology [1]. Bioinspired design does not however systematically lead to any positive change in the environmental footprint [2]. The majority of recent bioinspired structural or smart materials are based on the use of synthetic carbon fossil-based components, for which their life cycle impact is not considered in their design. This class of smart composites are used to convert environmental stimuli (like temperature) into a mechanical reversible deformation [3]. In this way, an actuation functionality is directly embedded in the microstructure of the material without using complex external devices [4]. Actuators based on those principles could therefore be autonomous, *i.e.* without requiring any external source of energy [5][6][7][8]. The natural environment is however complex, and a pure temperature variation may not be sufficient to guarantee actuation since temperature and humidity tend to superimpose their contributions. The actuation in biological systems is indeed triggered by the day-night cycle of the humidity combined with the change of temperature [9]. The coupled variation of humidity and temperature is rarely taken into account in the design of smart materials [10].

Biobased moisture-induced (hygromorph) actuators have been produced using asymmetrical lay-up $[0°, 90°]_{ns}$ stacking sequences. These bilayer composite architectures are inspired from those existing in natural hydraulic actuators like pine cone scales. The actuation is triggered by the swelling of natural fibers and the differential swelling between the layers. These composites could be made using wood bilayers [11][12][13][14], paper [15], paper/polymer [16] and natural fibers reinforced polymer configurations [17][18][19][20][21][22]. HBCs based on thermoplastic polymers are particularly interesting for general manufacturing because of their suitability to complex shape forming by thermocompression and/or 3D/4D printing. These HBCs could also be recycled at their end of life. Targeted applications of hygromorph materials include morphing systems and deployable structures for soft robotics, sun shading or evapotranspiration membranes for zero consumption buildings [23][12][11]. A recent report claims that autonomous sun shading systems could reduce

building heat input by 90%, resulting in saving 80 Mt CO_2 per year [24].

HBCs are however a recently new development, and the characterization of their responsiveness over broad ranges of relative humidity has not been evaluated so far; papers existing in open literature tend to focus on the behavior during water immersion tests [17][18][19][20][21][22]. Full immersion trials provide very useful information to develop HBCs, but also cause specific degradation mechanisms such as oligo or polysaccharides leashing, which may not occur in conditions of relative humidity.

The present article aims to provide a comprehensive description of the effects caused by the relative moisture induced by the relative humidity RH and moisture content on the bending actuation performance of hygromorph biocomposite actuators. The first part of the article concerns the evaluation of the hygroscopic properties (i.e., sorption and hygroscopic expansion) of MAPP/flax unidirectional laminates, with a description of the moisture sorption mechanisms occurring in the composites. Flax fibers have been chosen in this study because of the availability of high quality flax reinforcement preforms (lightweight unidirectional tapes), and also in view of their moderate environmental footprint [25]. The mechanical behavior and the elastic properties of the biocomposite laminates have been then characterized under different loading cases (longitudinal or transverse tension, in-plane shear) as a function of the moisture content. This set of mechanical and sorption characteristics thus constitute a relatively large experimental database that enables the prediction of the actuation performance of these composites.

The second part of this paper is related to the simulation of the bending actuation performance of the HBCs. Analytical and numerical estimations based on the material characterization described in the first part of the article are compared to experiments. The importance of the hygromechanical properties as well as their dependence upon the geometrical parameters defining the composites are then discussed.

2 Materials and methods

2.1 Materials

Flax fibers (*Linum usitatissimum*) have been harvested in France and then dew-retted before being scotched and hackled. The unidirectional (UD) flax fibers tapes (200 g/m² and 50 g/m²) were supplied by Ecotechnilin. Extruded and film-cast polypropylene (PPC 3660 from Total Petrochemicals, 70g/m^2) and maleic anhydride compatibilized polypropylene (MAPP) are used to manufacture the MAPP/flax biocomposites laminates.

2.2 Manufacturing

Laminates with stacking sequences (0°, 90° and ± 45°) are manufactured by film stacking and by using a dedicated hot press moulding process (190°C for 8 min at 20 bar, with an incremental pressure applied to maintain the alignment of the fibers). The cooling rate used is 15°C/min. The samples have the following dimensions (thickness t and width w): $t_{0°}$ = 1 mm and width $w_{0°}$ = 15 mm; $t_{90°}$= 2 mm and $w_{90°}$=25 mm; $t_{\pm45°}$ = 2.45 mm with 32 plies and $w_{\pm45°}$ = 25 mm). The fiber content is 60% by volume [21]. The hygromorph biocomposite actuators are designed with a passive-to-active thickness ratio (*n*) of 0.2, which corresponds to the best curvature range previously observed for MAPP/flax HBCs [21]. Delamination issues between each layer are reduced by using the same polymer within the two layers.

Five coupons with dimensions of 70 mm × 10 mm are then cut to obtain specimens for the bending actuation experiments. By shaping the HBC with a high length-to-width ratio one can reduce the anticlastic curvature [26], which is difficult to predict with 1D models such as Timoshenko beams, and also approximately generate a cylinder as the actuated shape. These materials can also be used as a tool to evaluate the states of residual stress [27][28]. The composites are systematically dried in a vacuum oven at 60°C (assumed to be close to 0% RH) before characterization.

2.3 Mechanical characterization

The samples are stored prior testing in a vacuum oven until a constant weight is reached. This condition implies a minimal amount of water within the material, which is indicated here as 'zero' (i.e., anhydrous state). The samples are then placed in different moisture environments (10-30-50-70-90% RH), all regulated by specific salts and deionized water solutions. Some are also immersed in deionized water. The specimens are left in the moist or immersion atmospheres until their weight reaches a steady value. The mechanical properties of all specimens are determined by quasi-static tensile and shear tests according to the ISO 527-4 and ISO 14129 standards, using an Instron 5566 universal testing machine (cell load 10 kN). The cross-displacement used is 1 mm/min for the tensile tests, and 2 mm/min for in-plane shear ones. A constant temperature of 23°C is maintained during all the tests, and an environmental chamber (Secasi) provides the control of the relative humidity.

Two different types of test specimens are used: type A specimen (Unidirectional tape, fibers at 0°) and type B specimens (UD, fibers at 90°). These specimens are used to determine the longitudinal and transverse mechanical properties, respectively. The strain is measured with an extensometer during the longitudinal and the transverse tests. The tensile modulus is determined within a range of strains between 0.05 and 0.1 % according to the procedure suggested by Shah *et al.* [29]. Type C specimens ($[\pm 45]_{8S}$) are used to evaluate the in-plane shear properties. The shear stress and strain have been evaluated according to the ISO 14129 standard. A digital image correlation (Aramis 70Hz (3D Motion)) facility is used to track the strains during loading.

2.3.1 Moisture sorption and hygroscopic expansion

The moisture sorption during the transient and stationary states is assessed by using a Dynamic Vapor Sorption apparatus (DVS, from Hiden Isochema Ltd, UK). Sorption and desorption isotherms are obtained from the biocomposites with equilibrium moisture content (EMC) at 0;2;4;6;8;10;12 and

20. Intervals of 10% RH are recorded up to 90 RH% at each equilibrium set-point. The percentage gain M_t at any time t is calculated as:

$$M_t(\%) = \frac{W_t - W_0}{W_0}.100 \quad \text{(Eq. 1)}$$

In (1) M_t and W_0 are the weights of the sample after water exposure and of the dry material before sorption, respectively. All the data presented here are the average values from three replicated tests. Small samples of the composites (around 10 mg) are cut from the tensile specimen and placed inside the DVS. The humidity in the chamber is then maintained until the RH equilibrium set-point is reached. The samples are dried under vacuum before being exposed to a wet vapor increase; this has been done to obtain specimens with dry-weight baseline (assumed RH ≈ 0%) for the following mechanical testing. Water sorbed within the cell wall in natural fibers is fundamentally classified in two types: bound water (monolayer water) and free water (polylayer group). Bound water is an hydrate with a definite unit of the fibers molecule (OH groups for instance). Free water is not associated with OH groups, and it is mainly located in the microcapillaries (2-4 nm). To describe the behavior of the sorption in natural fibers or wood, the Hailwood & Horrobin (HH) solid-solution model has been extensively used [30]. For natural fibers the HH model enables to determine, during sorption, the concentration of the different types of water (monolayer M_h and polylayer M_s) by establishing a state of equilibrium between them [31]:

$$M = M_h + M_s = \frac{1800}{W}\left(\frac{K_1K_2H}{100+K_1K_2H}\right) + \frac{1800}{W}\left(\frac{K_2H}{100-K_2H}\right) \quad \text{(Eq 2)}$$

In (2), M is the percentage moisture content at a given percentage relative humidity (H), W is the molecular weight of the cell wall polymer per sorption site, and K_1 and K_2 are constants. The values of K_1 and K_2 are determined by plotting H/M against H. Further details are presented in [30] and [31]. To determine the water monolayer value, the method requires to monitor the sorption behavior at low RH values, thus justifying the use of the 2; 4; 6; 8; 10 and 12 % RH set-points.

It is possible to estimate the specific surface of the materials by assuming a Langmuir adsorption isotherm (low RH). One can also use the following estimate when the amount of water molecule covering the surface area of the adsorbent in a monolayer coverage (i.e., the asymptotic moisture content *MC* of the water monolayer M_h) and the volume occupied by a molecule in the monolayer are all known:

$$\text{Specific surface} = 3516 \times MC_{Mh} \quad \text{(Eq 3)}$$

The value 3516 is obtained by geometry estimations from the theoretical surface covered by one molecule of water [30]. The term MC_{Mh} represents the moisture content corresponding to the first water monolayer.

For each RH condition the hygroscopic dilatation is measured on five square shaped biocomposite samples with dimensions equal to 100 mm × 100 mm × 2 mm. To ensure that the measurements are all performed under similar conditions, three lines are plotted longitudinally and transversally to the fiber orientation on each sample. The markers allow the tracking of the evolution of the dimensions of the samples by using a caliper with an accuracy of 0.01 mm and a micrometer with an accuracy of 0.001 mm.

2.1.5 Hygromorph and bending curvature analysis

The bending curvature of the HBC (Fig. 1a) is evaluated during the variation of the moisture by periodically taking pictures of one side of the clamped sample (HD Pro c920 Logitech®, 15 Megapixels).

Each sample is fixed with a binder clip on a very small length of the sample to reduce the stress concentration over the bilayer, and therefore leaving a free length of approximately 60 mm. Image process analysis is performed using the ImageJ® software (National Institute of Health, USA). The

deformed shape is here assumed to be an arc of a circle, and the curvature is therefore measured by fitting the time-evolution of the sample to a 'circle' function (Fig.1b). The bending curvature (κ) is calculated according to the radius of the fitted circle.

2.3.2 Analytical and numerical modelling

The analytical solution of a beam subjected to bending due to the difference $\Delta\beta$ of the coefficients of hygroscopic expansion and the moisture content ΔM_t is given by Timoshenko [32], when only the longitudinal curvature is considered :

$$\Delta\kappa = \frac{\Delta\beta\Delta\mathrm{Mt}\ \mathrm{f}(m,n)}{\mathrm{h}} \quad \text{(Eq 4)}$$

$$\text{Where } f(m,n) = \frac{6(1+m)^2}{3(1+m)^2+(1+mn)\left(m^2+\frac{1}{mn}\right)} \quad \text{(Eq 5)}$$

In (4) and (5) $m=\frac{t_p}{t_a}$, where t_p and t_a represent the passive layer (0° layer) and the active layer (90° layer) thicknesses, respectively (Fig. 1a). The parameter n is equal to $\frac{E_p}{E_a}$, where E_p and E_a represent the tensile moduli along the beam length of the passive and active layers, respectively. The differential hygroscopic expansion coefficient along the beam length between the active β_a and passive β_p layer is represented by $\Delta\beta$. The term ΔMt is related to the change of moisture content in the HBC between RH_i and RH_{i+1} .

Finite element simulations of the bilayer behavior have been also performed using the commercial software Abaqus™ (version 6.10). The sample is taken in a vertical position z > 0 at 50% RH, and clamped at x=0. The geometry consists in a rectangle of height h = 60 mm and width w = 10 mm. The thickness of the bilayer is modeled by shell elements with Kirchoff-Love kinematics and plane stress conditions (classical laminate theory - CLT). The finite elements are rectangular with eight nodes and four integration points in their plane (reduced integration) and three integration points through-the-

thickness. The shell is meshed regularly with 100 (or 10,000 for checking convergence conditions) elements. Each layer is assumed to follow a transverse isotropic linear elastic behavior. The hygroexpansion is introduced like a transverse isotropy thermal expansion in the code, where stationary regime is assumed. Elastic properties and hygroscopic expansion parameters depend on the level of moisture in the layer. Finite strains and finite displacements are considered.

3 Results and discussions

3.1 Hygroscopic properties of the MAPP/flax laminates

3.1.1 Moisture sorption

Fig. 1c presents the relative evolution of the moisture content during sorption and desorption at steady state for the biocomposites and the flax fibers, compared to the maximum *MC*. The data show the clear contribution provided by the fibers within the biocomposite. Fig.1d shows the comparison between experimental and HH model sorption and desorption isotherms for the MAPP/flax biocomposites.

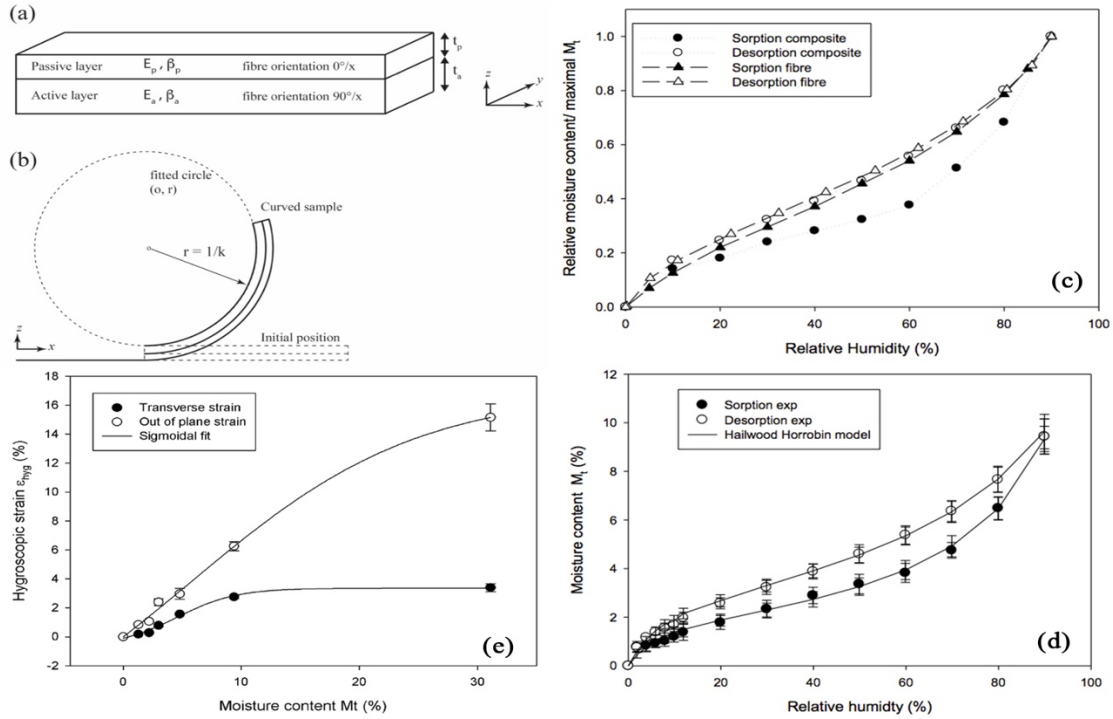

Figure 1 (a) Schematics of the biocomposite bilayer geometry. (b) Measurement of the bending curvature. (c) Relative moisture content changes during sorption and desorption behavior for the MAPP/flax biocomposites and the flax fibers. (d) Comparison between experiments and HH model for the MAPP/flax biocomposites. (e) Evolution of the transverse and out-of-plane swelling strains as a function of moisture content measured at steady state. The continuous lines represent sigmoidal fits.

Flax fibers are very sensitive to the moisture variation, and their sorption behavior is typically sigmoidal [33][31]. At low RHs (<10%) the water is sorbed onto specific sites by hydrogen bonding. When the relative humidity increases saturation of these specific sites occurs because of sorption. The water concentration then increases linearly with the relative humidity as per Henry's law (until RH ≈ 65%). This behavior is explained by the porosity present in the single and bundled fibers, in which water is free to diffuse. The third part of the curve is well described by a power function that represents the aggregation of the water molecules. At high relative humidity levels the water concentration is large, and the water molecules link together to form clusters.

The MAPP/flax biocomposites feature 60% flax fibers by volume, which corresponds to 70% in mass fraction. The sorption here appears similar to the one observed in flax fibers, with a sigmoidal behavior (Fig. 1c and d). MAPP/flax biocomposites show however a greater hysteresis loop than the one of the fibers alone (Fig. 1c). The hysteresis loop is typical of microporous media, and it is likely due to the evolution of the free volume within the material, *i.e.* the interfacial porosity created by the swelling and/or the shrinkage of the fibers and their bundles [34]. In addition, the water uptake generates large amounts of swelling stress [35], which in turns can explain the difference between the sorption and desorption mechanisms. The evolution of the mechanical properties of the polymer (plasticizing effect) could also be another reason behind the presence of the hysteresis loop. Salmen [36] emphasize the strong impact of the moisture content on the elastic properties of wood fibers walls. The variation of the mechanical properties is attributed in that case to the water molecules

acting as plasticizers, which enable to change the elastic stiffness of hemicellulose polymers (a fiber biopolymer with high oxygen/carbon ratio) by several decades of magnitude. Bast fibers [37] also show a bell-shaped dependency of the tensile modulus versus the water content (increase and then decrease) when subjected to quasi-static tests.

The HH model is applied here in the MAPP/flax biocomposites (Fig. 1d) by assuming that the contribution of the MAPP matrix to the moisture sorption is negligible due to the low surface energy. The HH model (Eq 2) fits very well the experimental data (Fig. 1d), and allows to estimate the contribution of the two types of water adsorbed. The monolayer water is present in the cell wall molecules, *i.e.* in flax fibers rich in polysaccharides (OH groups). The polylayer water is indicative of a transient state with microcapillarity networks, and with some water molecules engaged in hydrogen bonds with the water monolayer.

The values of monolayer (M_h) / polylayer (M_s) ratios are estimated from the HH model, *e.g.* 1.83 ± 0.23 % / 14.9 ± 2.0 %, and 2.87 ± 0.20 % / 9.94 ± 0.80 % for sorption and desorption respectively. Large differences are noticed between the M_h and M_s values, and these confirm the existence of the multiple steps process concerning the moisture sorption and transport. This process is still apparent even when the fibers are embedded in a fully hydrophobic thermoplastic matrix.

It is possible to estimate the specific area from the knowledge of the value of M_h and the volume occupied by a molecule in the monolayer (Eq 4). The cycle of desorption and loss of water induces a drastic 40% increase of the specific area (*e.g*. from 64.3± 8 to 101± 7 m²/g). This confirms the hysteretic sorption/desorption process due to evolution of the free volume.

A 90% of humidity leads to a weight increase of the biocomposite by 9.3%, which is three times lower than in the case observed in similar samples immersed in deionized water ($M_{t\ \text{immersion}}$ = 29. 9 ± 1.2 %). This difference is due to the free water transport. The presence of liquid water and a wet environment therefore imply a difference in the sorption responses of these MAPP/flax

biocomposites. In terms of potential applications like large scale smart bioinspired hygromorph actuators, a large weight increase due to the water uptake may reduce the overall efficiency of the bio device.

3.1.2 Hygroexpansion measurements

Natural fibers exhibit large anisotropic dimensional variations that depend upon the relative humidity (RH) and their moisture content [38]. At laminate scale (unidirectional ply) the moisture induces a monotonic increase of the swelling strains. These strains are orthotropic (Fig. 1e), and the longitudinal swelling strain (along the *x* axis, see Fig.1a) is too small to be measured correctly ($\varepsilon_{hyg,\,x} \approx 0$). On the opposite, the out-of-plane through-the-thickness strain $\varepsilon_{hyg,\,z}$ measured at steady state is significantly larger than $\varepsilon_{hyg,\,y}$, which is the transverse one (Fig. 1e) ($\varepsilon_{hyg,\,z} \approx 6.26 \pm 0.30$ % against $\varepsilon_{hyg,\,y} \approx 2.75 \pm 0.11$% at 90% RH, and $\varepsilon_{hyg,\,z} \approx 15.16 \pm 0.90$ % versus $\varepsilon_{hyg,\,y} \approx 3.40 \pm 0.30$ % in immersion). Moreover, the kinetics of the out-of-plane swelling strains is faster than the one of the transverse strains. A similar trend has been also observed on flax/polyester laminates manufactured by infusion [39]. Some likely explanations about these behaviors are provided by the effects of the geometrical constraint from neighboring fibers along the transverse direction, as well as by the presence of stress relaxation.

The actuation of the hygromorph biocomposites depends on differential hygroscopic strains within the bilayer microstructure. The control of the out-of-plane swelling could be an interesting way to enhance the responsiveness of HBCs. Its effect on the behavior of the hygromorph composites will be discussed in the following section.

From a general perspective, the behavior of the hygroscopic strains along the two *z* and *y* directions versus M_t are well described by a sigmoidal function with a high correlation ($R^2 = 0.99$) (Fig. 1e). For values of M_t between 0 and 10% , a quasi-linear relationship is observed ($R^2 = 0.964$ along *y* and, 0.985 along *z*) between ε_{hyg} and M_t, similarly to what has been observed at the fibers scale [38]. Within this

range, it is therefore possible to estimate a set of swelling parameters (β_z and β_y coefficients) that will be used as input data for the modelling of the actuation. Above M_t = 10%, one can notice that the transverse strains tend to reach a plateau, while the out-of-plane ones still have a linear dependence, followed by a softening with the moisture content (Fig. 1e). Thus, on the whole range $0 < M_t < 30\%$, the hygroscopic coefficient $\beta_{z,t}$ of the MAPP/flax biocomposites depends heavily on the moisture content, probably due to the evolution of the free volume fraction [40], the porosity located in the lumen [41], and the effects of the fibers/fibers and fibers/matrix interface. As mentioned above, other causes could also be related to the mechanical properties (plastic effects) and the hygroscopic stress state [42].

3.2 Evolution of the elastic properties

The elastic properties of the MAPP/flax biocomposites (longitudinal E_1, transverse E_2 and shear moduli G_{12}) are evaluated as a function of RH and the moisture content (Fig. 2a, b and c). Immersion tests have also been performed to generate the high moisture content. In summary (and as expected from classical laminate mechanics): the modulus E_1 depends mainly on the properties of the longitudinal fibers, while E_2 and G_{12} depend on the matrix and fiber/matrix interface.

Contrary to synthetic composites in which the longitudinal modulus is hardly affected by moisture due to the hygro stability of glass and carbon fibers [43][44], the Young's modulus E_1 in the MAPP/flax composites is drastically altered by the variation of moisture (Fig. 2a). This confirms previous observations made on flax composites within smaller intervals of RH values [45].

Similarly however to synthetic composites, the moduli E_2 and G_{12} decrease by almost 65% within the $0 < M_t < 10\%$ range, followed by a stabilization of the properties (Fig 2b and c). The longitudinal and transverse properties measured here show comparable exponential decays over the moisture content.

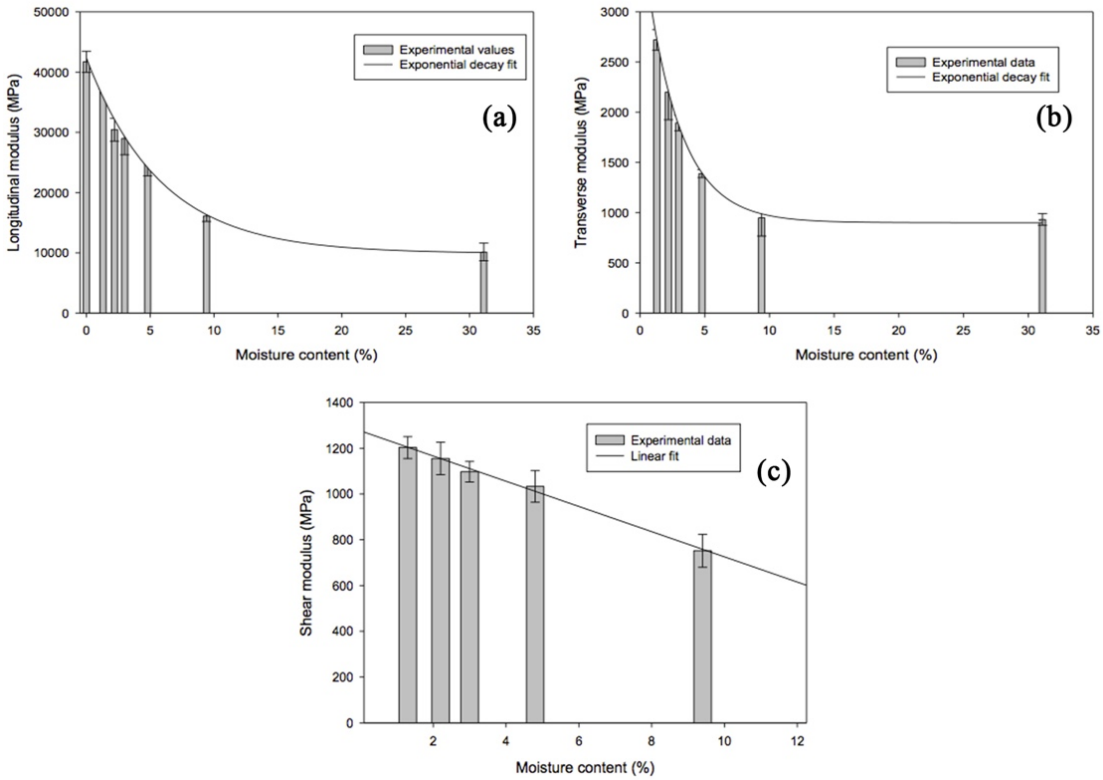

Figure 2 Evolution of the longitudinal modulus E_1 (a), transverse modulus E_2 (b) and Shear modulus G_{12} (c) as a function of the moisture content (%).

The 90% RH and immersed samples were then subjected to drying, and an almost complete recovery of the elastic properties was obtained; this phenomenon emphasizes the presence of a plasticization mechanism, which basically results in a reversible moisture-induced softening effect [46]. By assuming that MAPP is almost insensitive to water, an increase of the moisture content reduces the longitudinal modulus of the fibers and alters the interfacial bond strength. This is confirmed by studies at different scales (cell wall [47][48], fibers [37] and fibers/matrix interface [47]). The decrease of the T_g of several fiber cell-walls with polysaccharides [49] is also often cited as another possible cause.

3.3 The hygromorph biocomposites (HBC)

3.3.1 Characterization of the actuation

HBCs exhibit as actuators a self-shaping bending response when a moisture variation is observed (Fig. 3a). This section describes with experiments and models the behavior of these bio-based composite actuators over a wide range of humidity variation and application of the actuation.

The curvature of the HBCs was evaluated from the measurement of the X-Y coordinates of the samples during sorption/desorption from 0% to 90% RH, and during water immersion (Fig. 3b). As the radius of curvature *r* is nearly constant along the length of the sample, the curvature (*k=1/r*) is calculated as a function of time to follow the amplitude and response time. The bilayer is almost straight at RH=50% and the curvature is nearly equal to zero. Residual stresses that combine thermal and hygroscopic stresses are then released. From this equilibrium position, the curvature of the HBC could be either positive (50-90% RH) or negative (0-50% RH).

The actuation behavior follows a common pattern in all the RH environments considered here (Fig. 3b). Initially, one can observe a rapid increase of the curvature, followed by a plateau in which maximal curvature is reached (Fig. 3c). The responsiveness of the HBC can be therefore defined as:

$$k_{Max} = k_{final} - k_{initial} \qquad \text{(Eq 6)}$$

In (6), $k_{initial}$ is the initial curvature at 0% RH (-0.026 ± 0.0015 mm^{-1}), and k_{final} is the curvature obtained at the stationary regime.

The responsiveness of the MAPP/flax HBC significantly depends upon the humidity range. The experimental data fit well an exponential dependence (R^2=0.98, Fig. 3d), in which k_{max} at 90% RH is doubled compared to the analogous value at 50% RH; this is explained by the moisture sorption and the swelling behavior (Fig. 1c, d and e). If a large HBC deployment is targeted, a humidity lower than 50% would not provide an efficient deploying actuation, and variations within the 50-90% RH range should be instead preferred. It is also worth of notice that these hygromorph actuators are currently

manufactured using an apolar MAPP matrix and flax fibers. The use of a moisture-sensitive polymer could however provide wider actuation ranges. The responsiveness of the HBC exhibits a relationship with the moisture content that follows a sigmoidal function. This behavior may be divided into an almost linear trend at moistures lower than 10%, followed by a stabilization (Fig. 3e). When measured in immersion, k_{Max} is around 30% higher than k_{Max} at the 90% RH case, while the immersion M_t is 300% higher than at 90 % RH (Fig. 1d). This can be explained by the evolution of the hygroscopic strains $\varepsilon_{hyg,\,y}$ (Fig. 1e), which is strictly correlated to the water accumulation in the free volumes, the softening of the polymers and the presence of defects.

The responsiveness depends on the hygro-elastic strains due to anisotropic swelling ability of the flax composites beyond the moisture content present in the laminate. The swelling of the natural fibers and their laminates is therefore the key factor to develop high-performing biocomposite actuators.

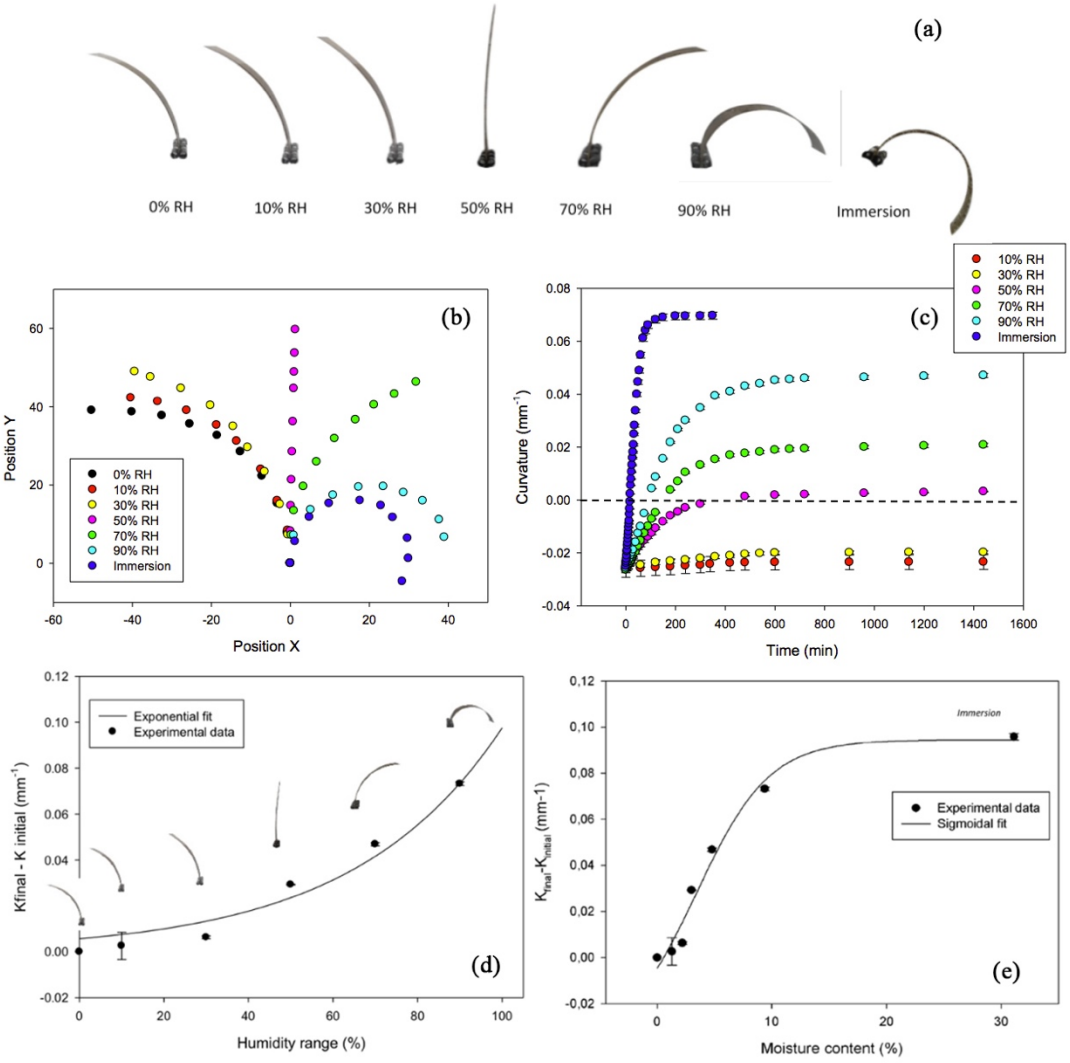

Figure 3 (a) Pictures exhibiting the evolution of the shape of a hygromorph biocomposite as a function of the environmental conditions (relative humidity and immersion). (b) Examples of X-Y plots at stationary regimes of the hygromorph biocomposite; (c) curvature of the HBCs as a function of time. Evolution of HBC responsiveness as a function of (d) humidity range and (e) moisture content.

The reactivity or actuation speed of the HBCs is determined from the initial slope of the curvature as a function of the actuation time (Fig. 3c). For this reason, it could not be presented as a function of the single moisture content, but rather of a moisture content range.

Reactivity is increasing monotonically with RH with a bilinear behavior (Fig. 4a). The change in slope is located at around RH = 30%, which corresponds to the beginning of the plasticization of the polysaccharides, lignin, pectin and hemicellulose in the flax fibers [41][49]. The reactivity then

accelerates sharply, in a similar way to the responsiveness (Fig. 3d). During the immersion the actuation speed is fivefold compared to the case at 90% RH. At 90% RH moisture clustering happens through capillary condensation. On the opposite, when the sample is immersed, the water is in a liquid state, and capillarity is directly activated. By increasing the moisture gradient, *i.e.* with larger humidity ranges (from 0 to RH), it is therefore possible to facilitate the transport of moisture within the biocomposite actuator.

There results show again that higher humidity levels (> 50%) should be adopted to make an efficient use of the MAPP/flax HBCs.

Similarly to wood bilayer types, hygromorph biocomposite actuators could also be used in evapotranspiration cladding or membranes [11][12][23], shading [50], soft robotics systems [51] or more generally for morphing structures. For those applications, the reversibility of the actuation during the sorption/desorption cycles is a key factor to their efficiency.

The reversibility trails have been performed by using the following protocol. The samples have been stored at 10 % RH until their saturation weight was reached. The specimens have then been moved in a 90% RH chamber, and their actuation characterized (Fig. 4b). The 90% RH saturated samples have then been dried to 10 % RH (Fig. 4b), followed by the application of incremental humidity loads (from 0 to 10, 30, 50, 70 and 90 % RH and then drying - Fig. 4c).

The first observation is related to the full reversibility of the MAPP/flax HBC samples during this sorption/desorption cycle. Thus, when the stimulus is removed the system returns automatically back to its lower energy state. The moisture-induced damages (matrix, fibers/matrix cracking) due to the internal stress state within the asymmetric laminate are therefore limited.

During the desorption (Fig. 4b) the MAPP/flax actuators show a hysteretic behavior that has already been observed from the sorption measurements (Figs. 1c and d). Unlike the case of cyclic immersion tests published elsewhere [21][22], here we notice a faster straightening during desorption

compared to bending during sorption (2.9 10^{-4} against 5.8 10^{-4} $mm^{-1}.min^{-1}$). The application of incremental humidity levels (Fig. 4c) confirms the presence of a fully reversible actuation behavior of these MAPP/flax HBCs on a wide range of RH values.

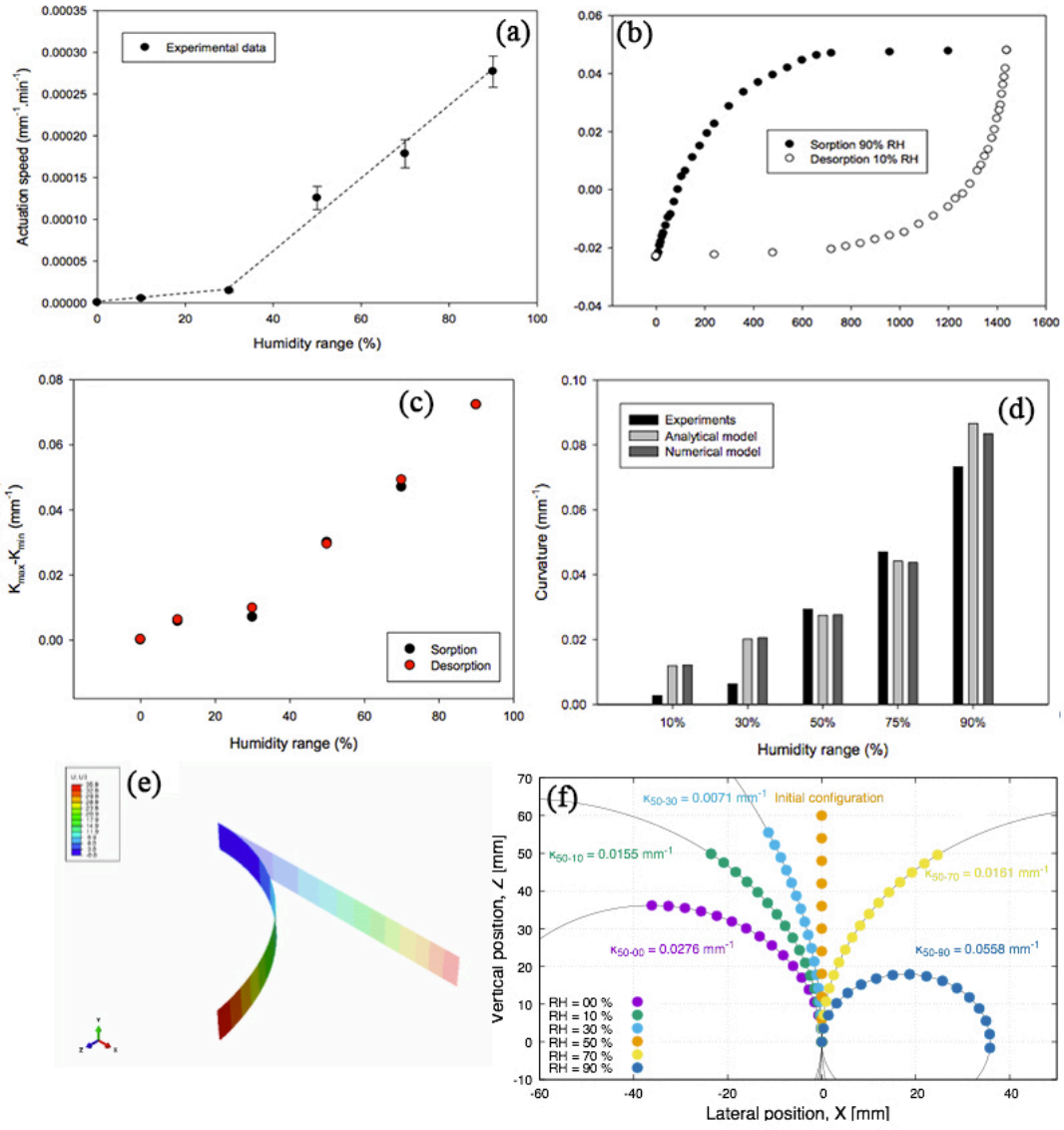

Figure 4 (a) Actuation speed (or reactivity) of a HBC as a function of humidity range. (b) Evolution of the curvature as a function of time (sorption from 10 to 90% RH and desorption from 90% RH to 10% RH). (c) Change of curvature at steady state as a function of the relative humidity. (d) Evolution of curvature from experimental data, analytical and numerical models, (e) Example of numerical displacement, (f) Curvature obtained by numerical simulation.

3.3.2 Morphing behavior

The HBCs considered in this work have a slender geometry (length to width ratio of 7), with an asymmetrical bilayer stacking sequence and specific *n* ratio (t_p/t_a = 0.2 [21]). The theoretical values of the curvature are calculated using the Timoshenko bimetallic model with experimental data as an input (Table S1, supplementary information), and compared to the experimental values (Fig. 4d).

A similar trend to the responsiveness is observed here for medium to high RH values (50-90% RH), with a slight (≈ 8%) underestimate for 50 < RH < 75%, and a 14% overestimate at RH=90%. Some more significant discrepancies are however observed at low RH (10-30% RH), with differences from 215 to 350 % (Fig. 4d). The modified Timoshenko model assumes a longitudinal curvature, and the effects of the Poisson's coefficients and the anisotropic properties of the MAPP/flax laminates (*i.e.* the transverse curvature) are not taken into account. No boundary condition effects such as clamping are also considered, and displacements significantly higher than the laminate thickness are present. From the above considerations it is therefore evident that the assumptions of the Euler-Bernoulli beam theory underpinning the Timoshenko are not satisfied here, hence we use a more complex finite element model based on classical laminate theory. Plane stress conditions are applied for the laminate plies and nonlinear geometric deformations are also considered. Nevertheless, the numerical results are within the same range of those provided by the analytical model (Fig. 4d). The slender geometry and the value of the passive to active thickness ratio imply that the transverse curvature effects are truly negligible (Fig. 4e).

During the simulations two major assumptions have been made. The first is that only the transverse isotropic swelling is considered. This is a very strong assumption, because the out-of-plane hygroscopic strains could be up to four times higher than transverse ones (Fig. 1e). However, by using the analytical model and modifying the overall thickness *t* with the out-of-plane hygroscopic strains ($\varepsilon_{hyg,\,Z}$ = 6.26 ± 0.30 %) one obtains results only slightly different from the theoretical ones (Fig. 4f).

The second assumption is that the β hygroscopic coefficients are assumed to be constant. This is not however what the experiments have shown here (Fig. 1e), because a sigmoidal function fits better the experimental data than a linear regression one ($R^2_{sigmoid}$ = 0.99, while R^2_{linear} =0.964). The use of the sigmoid function allows to reduce drastically the difference between the analytical model and the experimental results, especially at low RHs (Fig. 5a). Discrepancies however still remain for RH values below 50%, and this would need future further investigations.

3.3.3 Influence of the geometrical parameters

The finite element model developed in the previous section is now used to estimate the influence of geometrical parameters such as the slender ratio of the laminate (*length to width* ratio) and the *m* ratio on the response of the bending actuator. For the latter we have considered three thicknesses of the active ply: t_a = 0.391 mm, 0.156 mm and 0.078 mm, with thickness ratios $m = t_p/t_a$ = 0.2 (the experimental configuration), 0.5, and 1, respectively. Slenderness aspect ratios between 0.1 and 10 are considered in this work. The results are shown in Fig. 5b, and they clearly indicate that the curvature depends solely and linearly on the moisture content in the laminate, no matter which values of the aspect and thickness ratios are used. Moreover, for a given moisture content the higher curvatures values are found for the smallest thickness ratio considered here (0.5, with t_a = 0.156 mm).

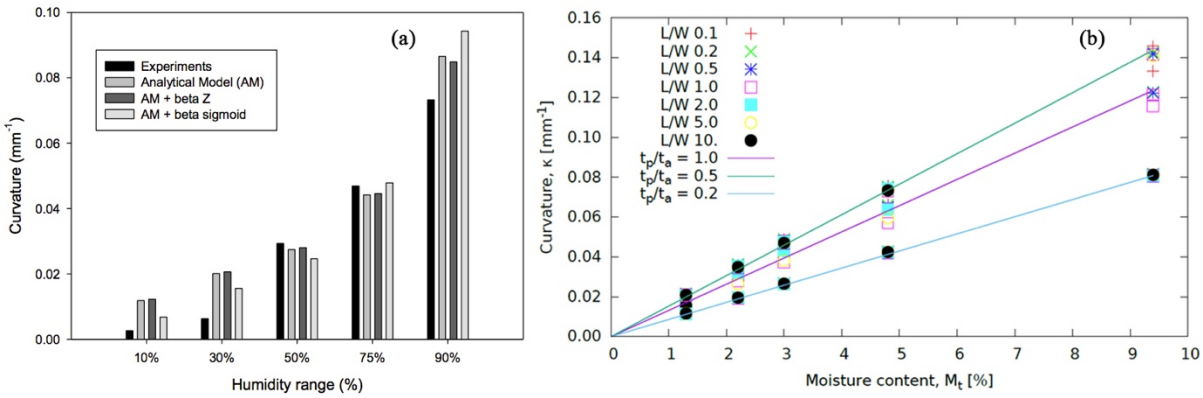

Figure 5 (a) Modification of the analytical model with the out of plane swelling (β_Z) and the use of a sigmoidal curve for β_y. (b) Curvature of the bending actuator as a function of the moisture content for the 7 aspect ratios (L/W) and three thickness ratios (t_p/t_a) considered in this work.

4- Conclusion

The objective of this work was building an experimental and modelling database to describe the moisture-induced actuation of bioinspired natural fibers composites hygromorph biocomposites (HBC). Hygro-mechanical experiments have been performed on unidirectional composites and asymmetric lay-up (bilayer) specimens and compared to simulations carried out with analytical and numerical simulation tools.

Similarly to what occurs in natural hydraulic actuators such as pine cones, the actuation on MAPP/flax hygromorph biocomposites is caused and limited by moisture sorption and transport. Sorption at the HBCs scale is comparable to the one present in flax fibers, which is well represented by the use of the HH model that underpins a multi-step process of moisture sorption and transport.

The hygroscopic coefficient of the MAPP/flax biocomposites depends on the moisture content, and features a trend similar to the one observed for the HBC responsiveness. This suggests that the actuation in HBCs depends on a hierarchical sorption/swelling mechanism. The sorption and swelling could be controlled by a multiscale interaction between the free volume fraction in the fibers lumen, and the fibers/fibers and fibers/matrix interfaces during sorption. In addition, the constraining effect of the matrix and the adjacent plies would provide a plasticizing effect, as well as the creation of hygroscopic stresses. This could also play a role in the overall sorption/swelling process of the biocomposite. The HBCs exhibit promising shape change and reactivity within the whole interval of relative humidity considered (10-90% RH), with a change of sign of curvature at 50% RH ($Mt \approx 3\%$). An acceleration of the actuation is observed as soon as the value of 30% RH is reached. Environmental conditions that involve a variation of moisture between 50-90% RH appear to provide the best efficiency in these MAPP/flax HBCs. Similarly to previous results in open literature related to full immersion tests, the relationship between the shape change and the moisture content does not

show a clear dependence. A sigmoidal behavior however fits well the experimental data, and that implies that a multi-step actuation process occurs in these biocomposites.

Both an analytical model based on modified Timoshenko equations and a classical laminate theory finite element one provide correct estimations of the curvature, especially between 50-90% RH. Below a relative humidity of 50% the two models do however fail to reach acceptable agreements with the experimental data. Further investigations about sorption, swelling and subsequent hygroscopic stress states will be required to develop satisfying predicting tools over broad humidity ranges. The numerical simulations have also highlighted that the slenderness of these biocomposites has no influence on their shape change characteristics, which opens multiple design opportunities.

Acknowledgements

The authors wish to thank CNRS for PEPS funding's, Ecotechnilin for materials providing and Ali Mellouki for his involvement at the beginning of this work.

5- References

[1] Chen J, Zhang X, Okabe Y, Saito K, Guo Z, Pan L. The deformation mode and strengthening mechanism of compression in the beetle elytron plate. Mater Des 2017;131:481–6. doi:10.1016/j.matdes.2017.06.014.

[2] Durand H, Larrieu C, Hubert C. Étude sur la contribution du biomimétisme à la transition vers une économie verte en France : état des lieux, potentiel, leviers. Http://WwwDeveloppement-DurableGouvFr/IMG/Pdf/ED72Pdf 2012.

[3] Wang Q, Tian X, Huang L, Li D, Malakhov A V., Polilov AN. Programmable morphing composites with embedded continuous fibers by 4D printing. Mater Des 2018;155:404–13. doi:10.1016/j.matdes.2018.06.027.

[4] Liu W, Chen H, Ge M, Ni Q-Q, Gao Q. Electroactive shape memory composites with TiO 2

whiskers for switching an electrical circuit. Mater Des 2018;143:196–203. doi:10.1016/j.matdes.2018.02.005.

[5] Kim SH, Kwon CH, Park K, Mun TJ, Lepró X, Baughman RH, et al. Bio-inspired, Moisture-Powered Hybrid Carbon Nanotube Yarn Muscles. Sci Rep 2016;6:23016. doi:10.1038/srep23016.

[6] Van Opdenbosch D, Fritz-Popovski G, Wagermaier W, Paris O, Zollfrank C. Moisture-Driven Ceramic Bilayer Actuators from a Biotemplating Approach. Adv Mater 2016;28:5235–40. doi:10.1002/adma.201600117.

[7] Mu J, Hou C, Zhu B, Wang H, Li Y, Zhang Q. A multi-responsive water-driven actuator with instant and powerful performance for versatile applications. Sci Rep 2015;5:9503. doi:10.1038/srep09503.

[8] Lee S-W, Prosser JH, Purohit PK, Lee D. Bioinspired Hygromorphic Actuator Exhibiting Controlled Locomotion. ACS Macro Lett 2013;2:960–5. doi:10.1021/mz400439a.

[9] Burgert I, Fratzl P. Actuation systems in plants as prototypes for bioinspired devices. Philos Trans R Soc A Math Phys Eng Sci 2009;367:1541–57.

[10] Etches J, Potter K, Weaver P, Bond I. Environmental effects on thermally induced multistability in unsymmetric composite laminates. Compos Part A Appl Sci Manuf 2009;40:1240–7. doi:10.1016/j.compositesa.2009.05.018.

[11] Reichert S, Menges A, Correa D. Meteorosensitive architecture: Biomimetic building skins based on materially embedded and hygroscopically enabled responsiveness. Comput Des 2015;60:50–69. doi:10.1016/j.cad.2014.02.010.

[12] Holstov A, Bridgens B, Farmer G. Hygromorphic materials for sustainable responsive architecture. Constr Build Mater 2015;98:570–82. doi:10.1016/j.conbuildmat.2015.08.136.

[13] Rüggeberg M, Burgert I. Bio-Inspired Wooden Actuators for Large Scale Applications. PLoS One

2015;10:e0120718. doi:10.1371/journal.pone.0120718.

[14] Burgert I, Eder M, Gierlinger N, Fratzl P. Tensile and compressive stresses in tracheids are induced by swelling based on geometrical constraints of the wood cell. Planta 2007;226:981–7. doi:10.1007/s00425-007-0544-9.

[15] Mulakkal MC, Seddon AM, Whittell G, Manners I, Trask RS. 4D fibrous materials: characterising the deployment of paper architectures. Smart Mater Struct 2016;25:095052. doi:10.1088/0964-1726/25/9/095052.

[16] Reyssat E, Mahadevan L. Hygromorphs: from pine cones to biomimetic bilayers. J R Soc Interface 2009;6:951–7. doi:10.1098/rsif.2009.0184.

[17] Correa D, Papadopoulou A, Guberan C, Jhaveri N, Reichert S, Menges A, et al. 3D printing wood :Programming hygroscopic material transformations. 3D Print Addit Manuf 2105;2:106–16.

[18] Le Duigou A, Castro M. Moisture-induced self-shaping flax-reinforced polypropylene biocomposite actuator. Ind Crops Prod 2015;71:1–6. doi:10.1016/j.indcrop.2015.03.077.

[19] Le Duigou A, Castro M. Evaluation of force generation mechanisms in natural, passive hydraulic actuators. Sci Rep 2016;6:18105. doi:10.1038/srep18105.

[20] Le Duigou A, Castro M, Bevan R, Martin N. 3D printing of wood fibre biocomposites: From mechanical to actuation functionality. Mater Des 2016;96:106–14. doi:10.1016/j.matdes.2016.02.018.

[21] Le Duigou A, Castro M. Hygromorph BioComposites: Effect of fibre content and interfacial strength on the actuation performances. Ind Crops Prod 2017;99:142–9. doi:10.1016/j.indcrop.2017.02.004.

[22] Le Duigou A, Requile S, Beaugrand J, Scarpa F, Castro M. Natural fibres actuators for smart bio-inspired hygromorph biocomposites. Smart Mater Struct 2017;26:125009. doi:10.1088/1361-

665X/aa9410.

[23] Ruggeberg M, Burgert I. Bio-inspired wooden actuators for large scale applications. PLoS One 2015;10:1–16.

[24] Piet Standaert (Physibel). ESCORP-EU25, Energy Savings and CO2 Reduction Potential from Solar Shading,. 2006.

[25] Duigou A Le, Davies P, Baley C. Replacement of Glass/Unsaturated Polyester Composites by Flax/PLLA Biocomposites: Is It Justified? J Biobased Mater Bioenergy 2011;5:466–82. doi:10.1166/jbmb.2011.1178.

[26] Alben S, Balakrisnan B, Smela E. Edge effects determine the direction of bilayer bending. Nano Lett 2011;11:2280–5. doi:10.1021/nl200473p.

[27] Gigliotti M, Jacquemin F, Molimard J, Vautrin A. Transient and cyclical hygrothermoelastic stress in laminated composite plates: Modelling and experimental assessment. Mech Mater 2007;39:729–45. doi:10.1016/j.mechmat.2006.12.006.

[28] Gigliotti M, Wisnom MR, Potter KD. Loss of bifurcation and multiple shapes of thin [0/90] unsymmetric composite plates subject to thermal stress. Compos Sci Technol 2004;64:109–28. doi:10.1016/S0266-3538(03)00213-6.

[29] Shah DU. Damage in biocomposites: Stiffness evolution of aligned plant fibre composites during monotonic and cyclic fatigue loading. Compos Part A Appl Sci Manuf 2016;83:160–8. doi:10.1016/j.compositesa.2015.09.008.

[30] Hailwood AJ, Horrobin S. Absorption of water by polymers: analysis in terms of a simple model. Trans Faraday Soc 1946;42:B084. doi:10.1039/tf946420b084.

[31] Hill CAS, Norton A, Newman G. The water vapor sorption behavior of natural fibers. J Appl Polym Sci 2009;112:1524–37. doi:10.1002/app.29725.

[32] Timoshenko S. Analysis of Bi-Metal Thermostats. J Opt Soc Am 1925;11:233.

doi:10.1364/JOSA.11.000233.

[33] Alix S, Lebrun L, Morvan C, Marais S. Study of water behaviour of chemically treated flax fibres-based composites: A way to approach the hydric interface. Compos Sci Technol 2011;71:893–9. doi:10.1016/j.compscitech.2011.02.004.

[34] Le Duigou A, Bourmaud A, Baley C. In-situ evaluation of flax fibre degradation during water ageing. Ind Crops Prod 2015;70:204–10. doi:10.1016/j.indcrop.2015.03.049.

[35] Peron M, Célino A, Castro M, Jacquemin F, Le Duigou A. Study of hygroscopic stresses in asymmetric biocomposite laminates. Compos Sci Technol n.d.

[36] Salmén L. Micromechanical understanding of the cell-wall structure. C R Biol 2004;327:873–80. doi:10.1016/j.crvi.2004.03.010.

[37] Placet V, Cisse O, Boubakar ML. Influence of environmental relative humidity on the tensile and rotational behaviour of hemp fibres. J Mater Sci 2012;47:3435–46. doi:10.1007/s10853-011-6191-3.

[38] le Duigou A, Merotte J, Bourmaud A, Davies P, Belhouli K, Baley C. Hygroscopic expansion: A key point to describe natural fibre/polymer matrix interface bond strength. Compos Sci Technol 2017;151:228–33. doi:10.1016/j.compscitech.2017.08.028.

[39] Testoni GA. In situ long-term durability analysis of biocomposites in the marine environment École nationale supérieure des mines de Paris I. Thesis Report- Mines Parit 2015.

[40] Adamson MJ. Thermal expansion and swelling of cured epoxy resin used in graphite/epoxy composite materials. J Mater Sci 1980;15:1736–45. doi:10.1007/BF00550593.

[41] Marklund E, Varna J. Modeling the hygroexpansion of aligned wood fiber composites. Compos Sci Technol 2009;69:1108–14. doi:10.1016/j.compscitech.2009.02.006.

[42] Sar BE, Fréour S, Davies P, Jacquemin F. Coupling moisture diffusion and internal mechanical states in polymers – A thermodynamical approach. Eur J Mech - A/Solids 2012;36:38–43.

doi:10.1016/j.euromechsol.2012.02.009.

[43] Arhant M, Le Gac P-Y, Le Gall M, Burtin C, Briançon C, Davies P. Effect of sea water and humidity on the tensile and compressive properties of carbon-polyamide 6 laminates. Compos Part A Appl Sci Manuf 2016;91:250–61. doi:10.1016/j.compositesa.2016.10.012.

[44] Tual N. Durability of carbon/epoxy composites for tidal turbine blade applications. 2015.

[45] Berges M, Léger R, Placet V, Person V, Corn S, Gabrion X, et al. Influence of moisture uptake on the static, cyclic and dynamic behaviour of unidirectional flax fibre-reinforced epoxy laminates. Compos Part A Appl Sci Manuf 2016;88:165–77. doi:10.1016/j.compositesa.2016.05.029.

[46] Davies P, Rajapakse YDS, editors. Durability of Composites in a Marine Environment 2. vol. 245. Cham: Springer International Publishing; 2018. doi:10.1007/978-3-319-65145-3.

[47] Le Duigou A, Davies P, Baley C. Exploring durability of interfaces in flax fibre/epoxy micro-composites. Compos Part A Appl Sci Manuf 2013;48:121–8. doi:10.1016/j.compositesa.2013.01.010.

[48] le Duigou A, Bourmaud A, Balnois E, Davies P, Baley C. Improving the interfacial properties between flax fibres and PLLA by a water fibre treatment and drying cycle. Ind Crops Prod 2012;39:31–9. doi:10.1016/j.indcrop.2012.02.001.

[49] Basu S, Shivhare US, Mujumdar AS. Moisture adsorption isotherms and glass transition temperature of xanthan gum. Dry Technol 2007;25:1577–82. doi:10.1080/07373930701539795.

[50] Vailati C, Bachtiar E, Hass P, Burgert I, Rüggeberg M. An autonomous shading system based on coupled wood bilayer elements. Energy Build 2018;158:1013–22. doi:10.1016/j.enbuild.2017.10.042.

[51] Li S, Wang KW. Plant-inspired adaptive structures and materials for morphing and actuation:

a review. Bioinspir Biomim 2016;12:011001. doi:10.1088/1748-3190/12/1/011001.